Systematic Mutational Mapping of Sites on Human Interferon-β-1a That Are Important for Receptor Binding and Functional Activity

Laura Runkel, Carole deDios, Michael Karpusas, Matthew Betzenhauser, Celine Muldowney, Mohammad Zafari, Christopher D. Benjamin, Stephan Miller, Paula S. Hochman, and Adrian Whitty*

Biogen, Inc., 14 Cambridge Center, Cambridge, Massachusetts 02142

Received July 15, 1999; Revised Manuscript Received November 17, 1999

ABSTRACT: A systematic mutational analysis of human interferon-β-1a (IFN-β) was performed to identify regions on the surface of the molecule that are important for receptor binding and for functional activity. The crystal structure of IFN-β-1a was used to design a panel of 15 mutant proteins, in each of which a contiguous group of 2−8 surface residues was mutated, in most instances to alanine. The mutants were analyzed for activity in vitro in antiviral and in antiproliferation assays, and for their ability to bind to the type I IFN (ifnar1/ifnar2) receptor on Daudi cells and to a soluble ifnar2 fusion protein (ifnar2-Fc). Abolition of binding to ifnar2-Fc for mutants A2, AB1, AB2, and E established that the ifnar2 binding site on IFN-β comprises parts of the *A* helix, the *AB* loop, and the *E* helix. Mutations in these areas, which together define a contiguous patch of the IFN-β surface, also resulted in reduced affinity for binding to the receptor on cells and in reductions in activity of 5−50-fold in functional assays. A second receptor interaction site, concluded to be the ifnar1 binding site, was identified on the opposite face of the molecule. Mutations in this region, which encompasses parts of the *B*, *C*, and *D* helices and the *DE* loop, resulted in disparate effects on receptor binding and on functional activity. Analysis of antiproliferation activity as a function of the level of receptor occupancy allowed mutational effects on receptor activation to be distinguished from effects on receptor binding. The results suggest that the binding energy from interaction of IFN-β with ifnar2 serves mainly to stabilize the bound IFN/receptor complex, whereas the binding energy generated by interaction of certain regions of IFN-β with ifnar1 is not fully expressed in the observed affinity of binding but instead serves to selectively stabilize activated states of the receptor.

The type I interferons (IFNs)[1] mediate a wide range of biological effects (*1*). Their actions on cells include induction of resistance to viral infections, inhibition of proliferation of normal and transformed cells, and regulation of the differentiation state of immune system cells and modulation of their functions (*2*). The human type I IFNs comprise 12 IFN-α isotypes, 1 IFN-β, and 1 IFN-ω (*3, 4*). These proteins are related members of the helical cytokine family, and share varying degrees of sequence homology ranging from ∼80% sequence identity among human IFN-α isotypes to ∼50% sequence identity between a consensus IFN-α sequence and human IFN-β (*3, 5*).

All of the known effects of the type I IFNs are believed to be mediated through interaction with a common type I IFN receptor comprising two proteins, ifnar1 (*6*) and ifnar2 (*7*−*9*). Both ifnar chains have been categorized as class II cytokine receptors (*10*), based on sequence alignments and predictions of conserved structural elements (*11*). This family includes the receptors for IFN-γ (*12*), tissue factor (*13*), and IL-10 (*14*). Through their cytoplasmic domains, the ifnar1 and ifnar2 receptor chains associate noncovalently with the Janus kinases tyk2 (*15*) and jak1 (*7, 16*). Signaling occurs through activation of the STAT pathway (reviewed in *17*), as well as through activation of other known signaling pathways (*18, 19*), and culminates in altered patterns of gene expression (*20*). Ifnar1 and ifnar2 contribute to ligand binding to different extents. Heterologous cells transfected with the human ifnar2 chain alone bind IFNs with moderate affinity ($K_D \sim 10^{-9}$ M) (*21, 22*). The human ifnar1 chain alone does not bind IFN with measurable affinity, but when cotransfected with human ifnar2 it increases by approximately 10-fold the affinity of the receptor complex for binding most type I IFNs, including IFN-β (*23*). Functionally, it has been suggested that ifnar1 mediates the differential responsiveness of cells to different type I interferons (*24, 25*).

A number of reports suggest that stimulation of cells by different type I IFNs leads to distinct biological responses (*26, 27*). Given the large number of ligands in this family, it is intriguing to consider how the functions of these proteins can be mediated through a common cell surface receptor comprising only two proteins. Several lines of evidence point to the likelihood that the mechanism by which subtype-

* To whom correspondence should be addressed. E-mail: Adrian_Whitty@Biogen.com.

[1] Abbreviations: ATCC, American Type Culture Collection; DMEM, Dulbecco's modified Eagle's medium; EBNA, Epstein−Barr virus nuclear antigen; ELISA, enzyme-linked immunosorbent assay; EMCV, encephalomyocarditis virus; FACS, fluorescence-activated cell sorter; FBS, fetal bovine serum; hGH, human growth hormone; GH-R, hGH receptor; HBS, Hepes-buffered saline; hGHbp, hGH binding protein; his-tag, histidine tag; IFN, interferon; his-IFN-β, IFN-β containing an N-terminal histidine tag; ifnar, type I interferon receptor; ifnar2-Fc, extracellular domains of ifnar2 fused to the hinge, CH2, and CH3 domains of human IgG1; mAb, monoclonal antibody; PBS, phosphate-buffered saline; PVDF, polyvinylidenedifluoride; RU, response units; SPR, surface plasmon resonance; wt, wild type.

10.1021/bi991631c CCC: $19.00
Published on Web 02/16/2000

specific functional differences are transduced by the receptor involves alternative modes of receptor engagement, which result in alternative signaling potentials of the ligated receptor complex (*28*−*31*).

To elucidate the mechanism by which type I IFNs bind to and activate their receptor, detailed structure−activity studies are required. Currently, the three-dimensional crystal structures for four type I IFNs, murine IFN-β (*32*), human IFN-α-2b (*33*), human IFN-β-1a (*34*), and ovine IFN-τ (*35*), have been solved. While mutational analyses for some human IFN-α isotypes exist (reviewed in *36*), they predate the determination of the crystal structures of these molecules. Hence, in these studies it was not possible to design mutations based on any firm knowledge of the location of the mutated residue in the three-dimensional structure of the IFN molecule, or of its involvement in intramolecular interactions that are required for maintaining structural integrity.

To extend structure−activity studies to human IFN-β, we undertook the design and characterization of a panel of alanine substitution mutants, taking advantage of the availability of a high-resolution crystal structure of human IFN-β-1a (*34*), to allow a systematic, structure-based approach to mutant design. The goal of this investigation was to identify the residues of IFN-β that are important for receptor binding and biological activity, and to quantitatively correlate mutational effects on receptor binding with effects on function to obtain insights into how IFN-β interacts with and activates its receptor. The results of these studies led to the identification of distinct regions on the surface of human IFN-β that interact with ifnar1 and ifnar2, and to an analysis of the roles that specific interactions within these regions play in stabilizing the bound receptor complex and in bringing about receptor activation.

MATERIALS AND METHODS

Reagents and Antibodies. Recombinant (untagged) IFN-β was nonformulated AVONEX [human interferon-β-1a (IFN-β-1a), Biogen, Inc.]. Anti-IFN-β mAbs were obtained as follows: B-O2 was from Summit Pharmaceuticals, Fort Lee, NJ; the polyclonal antibodies anti-BG9418 and #447 and mAbs BIO2, BIO4, and BIO6 were from Biogen, Inc. (Cambridge, MA), and anti-IFN-β mAbs A7, B2, and B7 were generous gifts of Dr. Phillip Redlich and Professor Sidney Grossberg. The anti-ifnar1 mAb EA12 and other anti-ifnar1 and anti-ifnar2 mAbs were from Biogen, Inc.

Construction of IFN-β Alanine Substitution Mutants. The IFN-β gene was subcloned into plasmid pMJB107, a derivative of pACYC184 (*37*), in order to create silent mutations by site-directed mutagenesis (U.S.E. Mutagenesis Kit, Life Technologies, Gaithersburg, MD) which introduced unique restriction enzyme cleavage sites scattered across the gene. These unique restriction sites in the modified IFN-β gene were used to exchange wild-type protein coding sequences for synthetic oligonucleotide duplexes containing the mutated codons. Site-directed mutagenesis was also used to create two mutants, H91A/H97A and H121A, that carried discrete substitutions at only double and single amino acid positions, respectively. To obtain expression plasmids of the IFN-β genes, the modified genes were excised as a 761 base pair *Bam*HI−*Not*I fragment and subcloned into plasmid vector DSW247, which is a derivative of pCEP4 (Invitrogen, Carlsbad, CA) that lacks the EBNA1 gene. The EBNA 293 expression plasmids encoded mature IFN-β proteins downstream of and in protein coding frame with DNA sequences encoding the human vascular cell adhesion molecule-1 (VCAM-1) signal sequence (*38*), a six histidine tag followed by a three amino acid (SSG) spacer, and an enterokinase cleavage site (DDDDK). The DNA sequences of the recombinant plasmids were each confirmed.

Expression and Quantitation of IFN-β Alanine Substitution Mutants. The human EBNA 293 cells (*39*) were maintained as subconfluent cultures in Dulbecco's modified Eagle's medium (DMEM) supplemented with 10% fetal bovine serum (FBS), 4 mM L-glutamine, and 250 μg/mL Genetecin. The expression plasmids were transiently transfected into 10 cm^2 dishes of EBNA 293 cells using the lipofectamine protocol (Life Technologies, Gaithersburg, MD). Conditioned media were harvested 3−4 days posttransfection, cell debris was removed by centrifugation and filtration, and conditioned media were stored at 4 °C for up to 5 months. Western blots established that, for all of the mutants, the majority of the expressed protein was glycosylated. Although each protein contained an amino-terminal histidine-tag, purification of the mutant proteins proved unnecessary for the functional analyses since the expression levels were sufficient (0.5−100 μg/mL) to allow assays to be performed using unpurified proteins in conditioned media.

To quantitate his-IFN-β expression levels, ELISA assays were performed using polyclonal rabbit antibodies (anti-BG9418, Biogen, Inc.) to coat 96-well ELISA plates. A biotinylated form of anti-BG9418 was used as a secondary reagent to allow detection of IFN-β via streptavidin-conjugated horseradish peroxidase. A 1:1 dilution series (from 20 ng/mL to 0.15 ng/mL) of recombinant untagged IFN-β-1a [unformulated AVONEX, human interferon-β-1a (IFN-β-1a), Biogen, Inc.] was used to generate standard concentration curves for this assay. After two washes, the plates were developed using the peroxidase substrate tetramethylbenzidine. The absorbance at 450 nm was determined using an ELISA plate reader. The assay was most sensitive to IFN-β concentrations from 0.5 to 5 ng/mL. For ELISA assay, the conditioned media were diluted to obtain samples which would fall within this range. The concentration values measured by ELISA were confirmed by Western blot analysis. Conditioned media from the EBNA 293 cell cultures and IFN-β-1a standards were subjected to reducing SDS−PAGE on 10−20% gradient gels and blotted onto PVDF membranes. Immunoreactive bands were detected with another rabbit polyclonal IFN-β-1a-specific antiserum (#447, Biogen, Inc.), followed by treatment with horseradish peroxidase-linked donkey anti-rabbit IgG. Finally, additional Western blots were performed, loading equivalent amounts (based on the ELISA data) of each his-IFN-β (30 ng), showing that the immunoreactive bands obtained from blots probed with four different anti-IFN-β mAbs (BIO2, BIO4, BIO6, and A7), which recognize epitopes in distinct regions of the molecule, had comparable intensities.

To test whether the activities of purified and unpurified his-tagged IFN were equivalent, wt his-IFN-β and mutant proteins A1, A2, AB1, AB2, C2, CD1, CD2, D, and E were purified by nickel agarose affinity chromatography. The

purified preparations gave identical activities in cell-based binding and activity assays to the conditioned media for those mutants. The purified preparations of his-IFN-β proteins were also subjected to reducing gel electrophoresis followed by silver staining, to further verify ELISA and Western blot quantitation data of his-IFN-β expression levels. In these experiments, a dilution series of recombinant untagged IFN-β-1a (10, 20, and 100 ng) was included in the analysis to serve as a reference standard.

Surface Plasmon Resonance (BIAcore) Analysis. A BIAcore 2000 Biosensor system (Pharmacia−Amersham, Piscataway, NJ) was used to study the binding of the wt and mutant his-IFN-β proteins to the IFN-β-specific mAb B-O2 (Summit Pharmaceuticals, Fort Lee, NJ). Western blot analysis demonstrated that mAb B-O2 was unable to detect denatured IFN-β, indicating that B-O2 binds to a conformational epitope on IFN-β. Further support for this conclusion was derived from epitope mapping studies (ELISA and SPR experiments), which demonstrated that B-O2 has an extensive epitope, contributed by amino acid residues present in the *B*, *C*, and *D* helices (see Results; and Runkel, unpublished data). All experiments were performed at 25 °C at a flow rate of 10 μL/min, using HBS buffer (10 mM HEPES, 150 mM NaCl, 0.005% P20 surfactant, pH 7.4) containing 0.1 mg/mL bovine serum albumin. The same solution was used both as running buffer and as sample diluent. The CAB3 chip surface was activated with *N*-hydroxysuccinimide/*N*-ethyl-*N*′-(3-diethylaminopropyl)carbodiimide hydrochloride and then treated with mAb B-O2 (30 μL at 30 μg/mL in 10 mM acetic acid, pH 5.0). Residual activated sites on the chip were blocked with ethanolamine hydrochloride, pH 8.5. Treatment of the derivatized chip with 100 mM sodium bicarbonate, pH 9.0 (30 μL), followed by 200 mM sodium carbonate, pH 11.5 (30 μL), repeated 5 times, established a reproducible and stable base line. The final surface density of mAb B-O2 on the chip was 4000−5000 RUs.

To determine the binding properties of the his-IFN-β mutants to mAb B-O2, each mutant protein was injected over the chip surface at a concentration of 1 μg/mL (120 μL). The samples were prepared by diluting conditioned media containing the IFN-β mutants (or control media, or media containing 5 μg/mL IFN-β-1a) 5-fold with HBS. Immediately after each injection, the chip was washed with HBS buffer (600 μL). The increase in RUs resulting from binding of the his-IFN-β to mAb B-O2 was measured at the end of this wash cycle. The surface was regenerated between experiments with 30 μL of 100 mM sodium bicarbonate, pH 9.0, followed by 30 μL of 200 mM sodium carbonate, pH 11.5. After regeneration, the chip was equilibrated with the diluent buffer.

Construction of the Ifnar2-Fc Expression Plasmid and Preparation of Ifnar2-Fc. An expression plasmid for a fusion protein (ifnar2-Fc) consisting of the extracellular domain of the human ifnar2 (mature protein residues 1−243, GenBank L41943) and the hinge, CH2, and CH3 constant domains of human IgG1 was constructed in two steps as follows. The polymerase chain reaction (primers 5′-TCGTTAATTAAGCCGCCAGGATGCTTTTGAGCCAGAATG-3′, 5′-TTCGTCGACGCTAGCTTGAGAAGCTGC-3′) was used to amplify the human ifnar2 coding sequences (positions 1−243) from pBlueScript-ifnar2 (a gift from G. Uze, CNRS, Montpelier, France) and to incorporate suitable cloning sites for the DNA fragment (5′ site *Pac*I, 3′ site *Sal*I). This PCR fragment was cloned into expression plasmid pCA117 (Biogen, Inc.) using *Pac*I/*Sal*I restriction enzyme cleavage sites. Following digestion with *Kpn*I/*Sal*I, a fragment of the ifnar2 gene lacking the native signal sequence but containing the sequence encoding the entire extracellular domain was purified from the resulting plasmid, pIFNOV1. This fragment was subcloned into plasmid vector pCRFB4-CA117, between the CRFB-4 signal sequence (ending at the *Kpn*I site, GenBank U08988 and U12021) and the coding sequence for human IgG1 constant domain (starting at the *Sal*I site), to yield the final ifnar2-Fc expression plasmid pB4-ifnar2. The DNA sequence of this plasmid was confirmed. The fusion protein, ifnar2-Fc, was expressed following transient transfection of pB4-ifnar2 DNA into COS7 green monkey kidney cells. The ifnar2-Fc protein used in the IFN binding assays was purified by protein A−Sepharose chromatography from conditioned culture supernatants collected 3−4 days posttransfection.

Ifnar2-Fc:IFN-β Solid-Phase Binding Assay. To assess the binding properties of the his-IFN-β mutants to the extracellular domain of the human ifnar2 chain, a standard ELISA-based assay was performed as follows: Flat-bottomed, 96-well ELISA plates were coated with 50 μL of murine anti-human IgG1 mAb (10 μg/mL CD1G5-AA9, Biogen, Inc.) in coating buffer (50 mM $NaHCO_3$, 0.2 mM $MgCl_2$, 0.2 mM $CaCl_2$, pH 9.6) overnight at 4 °C. Plates were washed twice with PBS/0.05% Tween-20 (wash buffer) and blocked with 0.5% nonfat dry milk in PBS for 1 h at room temperature. After two washes, 50 μL of 1 μg/mL ifnar2-Fc diluted in 0.5% milk/PBS/0.05% Tween-20 was added to each well, and the plates were incubated for 1 h at room temperature. The plates were washed twice, and incubated for 2 h at 4 °C with 50 μL/well conditioned medium containing the appropriate his-IFN-β protein serially diluted in DMEM supplemented with 10% fetal bovine serum. The dilutions spanned an IFN concentration range from approximately 1 μM to 10 pM. The plates were washed, and bound IFN was detected by adding 50 μL/well of a cocktail consisting of a 1:1000 dilution of rabbit polyclonal antibody specific for human IFN-β-1a and horseradish peroxidase-conjugated donkey anti-rabbit IgG for 15 min at 4 °C. After two washes, the plates were developed using the peroxidase substrate tetramethylbenzidine, and the absorbance at 450 nm was determined using a SPECTRAmax PLUS plate reader. The absorbance was plotted as a function of IFN concentration, and EC_{50} values were determined graphically from the best fit of the binding curves to a hyperbolic equation.

Cell Surface Receptor Binding Assay. The cell surface receptor binding properties of the his-IFN-β mutants were assessed using a FACS-based assay which employed mAb EA12, an anti-ifnar1 mAb previously reported to block IFN-α2b binding to cells, signaling through STAT activation, and antiviral activity by blocking the interaction of IFN with the receptor (*40*). Preincubation of Daudi Burkitt's lymphoma cells with a range of IFN-β concentrations results in a concentration-dependent reduction in the subsequent binding of mAb EA12 that can be measured by flow cytometry (FACS) analysis. The standard protocol for a cell binding experiment utilized 20 μL of cells (2.5×10^7 cells/mL) and 20 μL of the his-IFN-β dilutions. All dilutions were made with FACS buffer (5% FBS, 0.1% NaN_3 in PBS). Cells and

IFN were incubated in 96-well, V-bottom ELISA plates for 1 h at 4 °C. Control experiments established that this incubation period was sufficient for IFN binding to reach equilibrium even at the lowest concentrations tested. Serial dilutions of IFNs gave final concentrations ranging from 0.5 μM to 0.5 pM. Cells then received 100 ng of biotinylated anti-ifnar1 mAb EA12 (10 μL) and were further incubated for 2 min at room temperature. Incubation with mAb EA12 was kept brief to minimize reequilibration of IFN-β binding. Unbound EA12 mAb was removed by two washes with FACS buffer (4 °C). The cells then were incubated with 50 μL/well of a 1:200 dilution of R-phycoerythrin-conjugated streptavidin for 30 min at 4 °C. The cells were washed twice in FACS buffer, resuspended in 300 μL of FACS buffer containing 0.5% paraformaldehyde, and transferred into 12 $\times$ 75 mM polystyrene tubes for subsequent analysis by flow cytometry. Mean fluorescence intensity was plotted as a function of IFN concentration for wt his-IFN-β and each of the mutant proteins. K_D values were given by the concentration of IFN-β that decreased binding of mAb EA12 by 50%, determined by performing a standard four-parameter curve fit on the data. In control FACS experiments, Daudi cells incubated with IFN-β as described above were treated with nonblocking anti-ifnar1 or anti-ifnar2 mAbs, in place of EA12, to demonstrate that there was no IFN-dependent loss of surface receptor (Su et al., unpublished data).

Antiviral Assay. Standard antiviral assays (*41*) were performed using A549 human lung carcinoma cells (ATCC CCL185). The cells were maintained in DMEM supplemented with 10% FBS and 4 mM L-glutamine. On the day prior to IFN treatment, the cells were seeded into 96-well, flat-bottom culture plates at a density of 3×10^5 cells/mL, using 100 μL of cell suspension/well, and allowing triplicate wells for each experimental point. On the next day, cells were treated with a range of IFN concentrations (for wt his-IFN-β, 100, 50, 25, 12.5, 6.25, 3.12, 1.56, and 0.75 pg/mL) for 20−24 h prior to challenge with encephalomyocarditis virus (EMCV) at a titer sufficient to lyse 100% of untreated cells. Two days after the addition of EMCV, viable cells were quantitated using the metabolic dye thiazolyl blue. A dye solution was freshly prepared in PBS (5 mg of thiazolyl blue/mL of PBS), and a 50 μL aliquot was added to each well. Following a room-temperature incubation (30−60 min), the supernatant was discarded, and the cells were washed with 100 μL of PBS. Finally, the cells were solubilized in 100 μL of 1.2 N hydrochloric acid in 90% 2-propanol. Viable cells were quantitated by measuring the absorbance at 450 nm. Some variation was seen between experiments in the sensitivity of the cellular response in antiviral assays; therefore, a full titration with wt his-IFN-β was included in each assay as a positive control. For his-IFN-β mutants with reduced specific activities relative to wt his-IFN-β, the optimal IFN concentration range was determined in pilot experiments using a wide range of IFN concentrations to identify concentrations sufficient to yield a full range of protection from viral infection under the conditions described above. The absorbance values were graphed as a function of his-IFN-β concentrations. An EC_{50} value, the concentration of IFN-β at which 50% of the cells were protected from viral killing, was determined from the graphs.

Antiproliferation Assays. Human Daudi Burkitt's lymphoma cells (ATCC CRL 7933) were seeded at 2×10^4 cells/well in a round-bottomed 96-well plate in RPMI 1620 supplemented with 10% defined fetal calf's serum and 4 mM L-glutamine and containing nine IFN concentrations derived from a 2-fold dilution series. For wt his-IFN-β, the concentration range used was from 2 ng/mL to 7.5 pg/mL. The IFN concentrations used for each of the his-IFN-β mutants were chosen based on pilot experiments to span a sufficiently broad range to define the concentration of mutant IFN required to achieve 50% growth inhibition. Duplicate experimental points were used, and a set of 6 wells/plate of untreated cells was included in all experiments to serve as a control to determine maximal thymidine incorporation values. Cells were incubated with the IFN at 37 °C in 5% CO_2 incubators for 2 days, after which 1 μCi per well of tritiated thymidine ([*methyl*-^{3}H]thymidine; Amersham, Arlington Heights, IL) was added in 50 μL of media. Following a further 4 h incubation, the cells were harvested using a plate harvester. Tritiated thymidine incorporation was measured using a beta plate reader. Duplicate experimental values were averaged and the standard deviations determined. Thymidine incorporation, as percent of maximum, was calculated for each IFN-β concentration, using 100% values determined from the untreated cells, and these values were plotted as a function of concentration. For each mutant, the IFN-β concentration required to achieve 50% growth inhibition (EC_{50}) was determined from the graphs.

RESULTS

Design of IFN-β Alanine Substitution Mutants. An approach based on alanine scanning mutagenesis was employed to identify the regions on the IFN-β surface that are important for receptor binding and for activity. Surface-exposed amino acids were mutated in groups of 2−8 residues to alanine or, in two positions, to serine. Mutations were designed with careful reference to the X-ray crystal structure of human IFN-β (*34*), to ensure that changes were restricted to residues with highly solvent-exposed side chains, and that residues with side chains involved in intramolecular interactions likely to be important for the stability of the folded structure were not altered. Glycine residues were not mutated, even when occurring at solvent-exposed positions, to avoid altering the geometry of the protein backbone. The solvent-exposed residues R27, R35, and K123 had been shown previously to be important for antiviral and reporter gene activities (*42*), and were therefore not altered in this study. Similarly, a mutation at position R124 had previously been shown to have no effect on activity (*42*), and was not included. Finally, residue T82 was mutated to a serine rather than to an alanine in order to preserve the glycosylation site at position N80, since glycosylation has been shown to be important for the stability and solubility of IFN-β (*43*). The structure of IFN-β contains 5 α-helices, designated *A*, *B*, *C*, *D*, and *E*, interconnected by loops of from 2 to 28 residues designated *AB*, *BC*, *CD*, and *DE* (*34*). Residues were mutated in 15 separate groups, shown in Figure 1, each of which was selected to define a more or less contiguous patch of the three-dimensional molecular surface. The mutants are designated A1−E, in accordance with the secondary structural element (helix or loop) in which the amino acid substitutions occur (Figure 1). The number of amino acid substitutions in each individual mutant ranged from 2 residues (mutants DE1 and DE2) to 8 residues (AB3), with most mutants containing

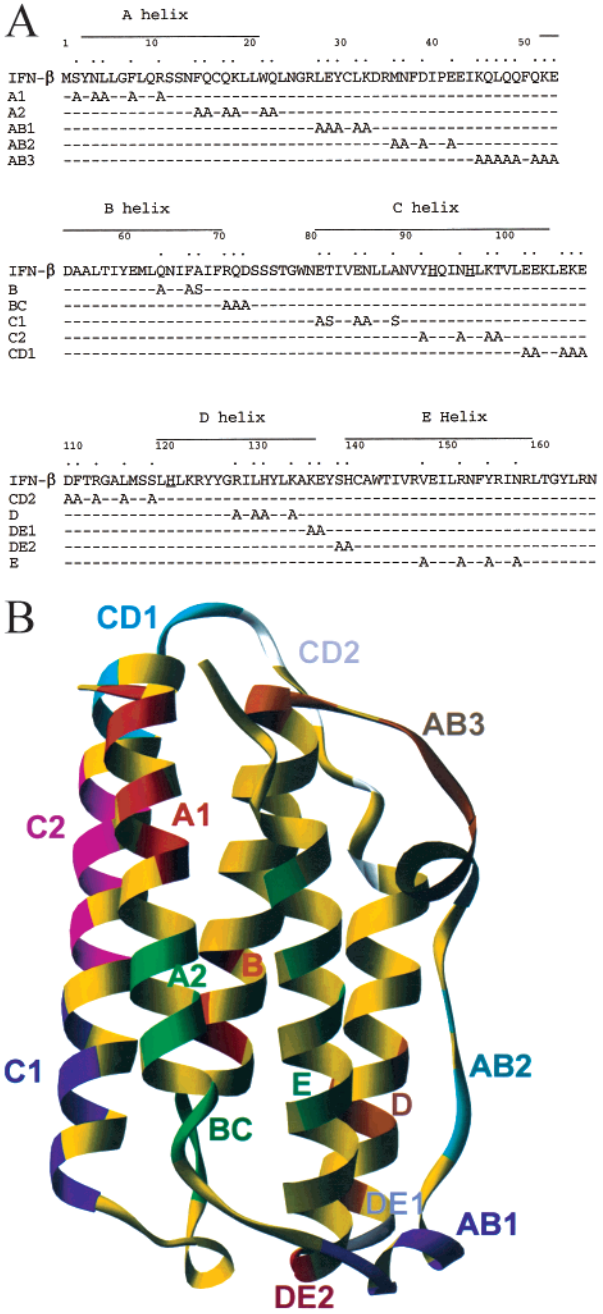

FIGURE 1: Locations of alanine substitution mutations in the primary, secondary, and tertiary structure of human IFN-β. (A) Locations of alanine substitution mutations in the primary sequence of mature human IFN-β-1a. The sequence of each mutant, A1−E, is shown below the section of wt IFN-β sequence in which the mutations occur. Dashes indicate that the mutant conforms to the wild-type sequence at that position, as it does at all other positions not shown. The locations of the 65 residues that were altered in the 15 mutants are shown by dots above the corresponding positions in the IFN-β sequence. The individual mutants are designated A1−E, in accordance with the secondary structural element (helix or loop) in which the amino acid substitutions occur. Two additional mutants were made, H93A/H97A and H121A (see text); these residues are underlined. (B) A ribbon diagram representation of IFN-β-1a with the locations of the mutations colored by group to show where they lie in the secondary and tertiary structure of the IFN-β molecule. Regions colored yellow correspond to unaltered residues. Figures were prepared using RIBBONS (*63*).

3−5 changes. The resulting panel of mutant proteins represents a low-resolution scan of essentially the entire surface of the protein, in which solvent-exposed amino acid side chains in successive regions of the protein surface have been removed. Altogether, 65 of a total of 166 residues in IFN-β were changed.

Expression and Characterization of IFN-β Mutants. The wt and mutant IFN-β proteins were expressed transiently in mammalian cells, to ensure glycosylation at N80. Each protein contained a 14-residue N-terminal extension, comprising a hexahistidine tag followed by an enterokinase cleavage site, upstream of the mature IFN-β protein sequence. Tests showed that enterokinase was not effective at removing the N-terminal his-tag from the wt his-IFN-β; stoichiometric concentrations of enzyme were required to achieve cleavage, and under these conditions additional cleavages in the IFN-β sequence were also observed. The specific activity of wt his-IFN-β was compared to that of untagged recombinant human IFN-β-1a in assays measuring the antiproliferative and antiviral activities of IFN-β, and was found to be comparable within a factor of 2−3 (data not shown). This result showed that the N-terminal tag present on the wt his-IFN-β did not substantially affect its activity in these assays. The proteins were found to be stable in the culture supernatant. Therefore, to facilitate the subsequent characterization of the mutant proteins, they were primarily tested as unpurified culture supernatants. The wt his-IFN-β and nine of the mutants were purified (Materials and Methods), and their antiviral and antiproliferation activities, as well as their receptor binding properties, were tested and in each case found to be indistinguishable from those of the corresponding unpurified protein.

Activity comparisons between wt his-IFN-β and the mutant proteins required that the concentration of each mutant present in the conditioned media be accurately known. IFN concentrations were measured by ELISA, and confirmed by Western blotting and also, for the 9 mutants which were purified, by silver-stained SDS−PAGE (data not shown). Standard curves were constructed using highly purified untagged recombinant human IFN-β-1a. The Western blot analyses were performed not only using a polyclonal anti-IFN-β antibody, but also separately with four different anti-IFN-β mAbs which recognize four distinct epitopes distributed within the IFN-β sequence in the *AB* and *CD* loops and in the *B* and *C* helices. This nonredundant panel of antibodies was used to rule out the possibility that quantitation using any one reagent might be affected if the antibody epitopes involved coincided with sites of mutation. The concentrations measured using these various methods were found to be in good agreement with each other (data not shown).

The structural integrity of the mutant proteins was investigated using three conformationally sensitive anti-IFN-β mAbs as probes. Figure 2 summarizes the results of two separate SPR experiments, which showed that most of the mutants bound to mAb B-O2 indistinguishably from wt his-IFN-β. Mutants BC and C1 did not bind to B-O2, however, and the binding of mutant C2 was substantially reduced (Figure 2). ELISA analysis confirmed that B-O2 does not recognize these three proteins (data not shown). As the mutations in BC, C1, and C2 affect contiguous regions of the IFN-β surface (Figure 1B), it was considered that these mutants might be correctly folded but that B-O2 binding might be altered due to its epitope lying in this region of the molecule. The structural integrity of these mutants was thus

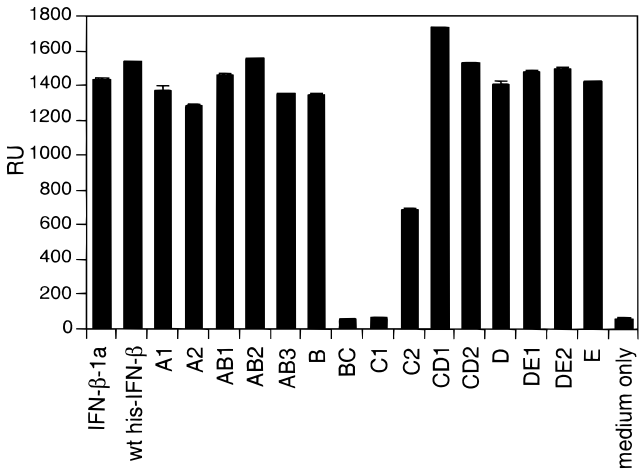

FIGURE 2: SPR analysis of the binding of mutants A1−E to the human IFN-β-specific mAb B-O2. Wild-type his-IFN-β and mutants A1−E were passed over a BIAcore chip to which mAb B-O2 had been covalently coupled, as described under Materials and Methods. Purified untagged recombinant IFN-β-1a in cell culture medium and no IFN-β (medium only) were included as positive and negative controls, respectively. The height of the bars (RU) represents the level of binding seen with the various his-IFN-β proteins tested. Each bar shows averaged data from two independent experiments; the error bars show the spread of the duplicate data points.

tested further by evaluating all of the mutants by ELISA for their ability to bind two additional mAbs, B2 and B7 (*44*), that bind a conformational epitope distant from that of B-O2. Their epitopes, located in the C-terminal portion of the *AB* loop and N-terminal portion of the *B* helix, lie on the opposite face of the IFN-β molecule to the B-O2 epitope. The results showed that mutants BC, C1, and C2 are recognized equivalently to wt his-IFN-β by these two conformationally sensitive mAbs (data not shown). The results obtained with the other mutants when tested using mAbs B2 and B7 confirmed the structural integrity of these proteins, with the expected exceptions that no binding was observed for mutants affecting regions of IFN-β that coincide with the previously published locations of the binding epitopes for mAbs B2 and B7 (*45*). Taken together, these data demonstrated that the mutations contained in the 15 IFN-β mutants shown in Figure 1 had only the desired local effects on the properties of the molecule, and did not disrupt the overall structural integrity of the protein.

Activity of IFN-β Mutants in Cell-Based Antiviral and Antiproliferation Assays. Activation of the type I IFN receptor is known to induce an antiviral state (*41*), and to inhibit cell proliferation in some cell types (*46*). These two effects are mediated by different sets of IFN-inducible genes, through at least partially distinct signaling pathways. In the assays we employed, 10-fold higher IFN concentrations were required to achieve 50% maximal activity in the antiproliferation assay compared to the antiviral assay, implying that the signaling responses that give rise to these two activities are sensitive to different levels of receptor occupancy. Because of the quantitative and qualitative differences between these two cellular responses to IFN-β, we chose to evaluate the activity of the his-IFN-β mutants in assays that measured each of these activities.

Antiviral activities of wt his-IFN-β and the 15 mutants were measured using A549 human lung carcinoma cells, which were pretreated with concentrations of IFN-β expected to span a full range of protection from killing by subsequent EMCV infection. The activity of each protein was defined as the concentration which resulted in 50% protection from viral killing in the assay, determined by interpolation of the dose−response data. Figure 3A shows representative data for wt his-IFN-β and for three mutants that span a range of antiviral activities. Data for each mutant were measured in at least three separate experiments, using proteins obtained from at least two separate transient transfections. A full dose−response curve with wt his-IFN-β was included in each assay. Figure 3B shows the antiviral activities obtained for each of the 15 mutants, represented as a percentage of the activity measured for wt his-IFN-β control in the same experiment. Each data point in Figure 3 represents the result obtained for a given mutant in a separate experiment; the mean percent activity for each mutant is shown by a horizontal bar. Figure 3B shows that mutants A1, AB3, B, C1, C2, CD1, CD2, D, and DE2 displayed antiviral activity that was essentially identical (i.e., within a factor of 2) to that of wt his-IFN-β. In contrast, mutations in the *A* helix (mutant A2), *AB* loop (mutants AB1 and AB2), the *BC* and *DE* loops (mutants BC and DE1, respectively), and the C-terminal portions of the *E* helix (mutant E) showed reductions in mean antiviral activity of from 4- to 50-fold.

The antiproliferation activity of the IFN-β mutants was determined by measuring their ability to inhibit the proliferation of Daudi Burkitt's lymphoma cells. Each protein was assayed at a range of concentrations, and its activity was defined as the concentration which resulted in 50% inhibition of [^{3}H]thymidine incorporation. Figure 3C shows representative antiproliferation dose−response data for wt his-IFN-β and for three mutants. As was the case for the antiviral assay, each mutant was assayed in at least three separate experiments, using proteins obtained from at least two separate transfections, and a full titration with wt his-IFN-β was included in each assay. Figure 3D shows the antiproliferation activities obtained for each of the 15 mutants, plotted as a percentage of the activity observed for wt his-IFN-β in the same experiment; the mean percent activity for each mutant is shown as a horizontal bar. Mutants A1, AB3, B, C1, C2, CD1, CD2, and DE2 displayed activity indistinguishable from that of wt his-IFN-β. Mutants A2, AB1, AB2, BC, D, DE1, and E showed mean antiproliferation activities that were reduced by factors of 5−25-fold compared to wt his-IFN-β.

It is immediately noticeable from comparison of Figures 3B and 3D that, with the exception of mutant D, the mutants that showed reduced activity in the antiproliferation assay are the same ones that showed reduced antiviral activity. The relationship between the effects of the mutations on these two distinct activities is examined more quantitatively in Figure 4, which shows antiviral activity plotted against antiproliferative activity (both expressed as a percentage of the activity of wt his-IFN-β control) for all 15 mutants. The solid line in Figure 4 has a slope of 1 and represents the relationship predicted for mutants that display identical effects on activity in the two assays. It is striking that the mutants, which collectively span more than 2 logarithms of activity, all fall on or close to this theoretical line. Closer examination of Figure 7 shows that mutants B, C1, D, and DE1 show mean antiproliferation activities that appear disproportionately lower, to a modest degree, than their

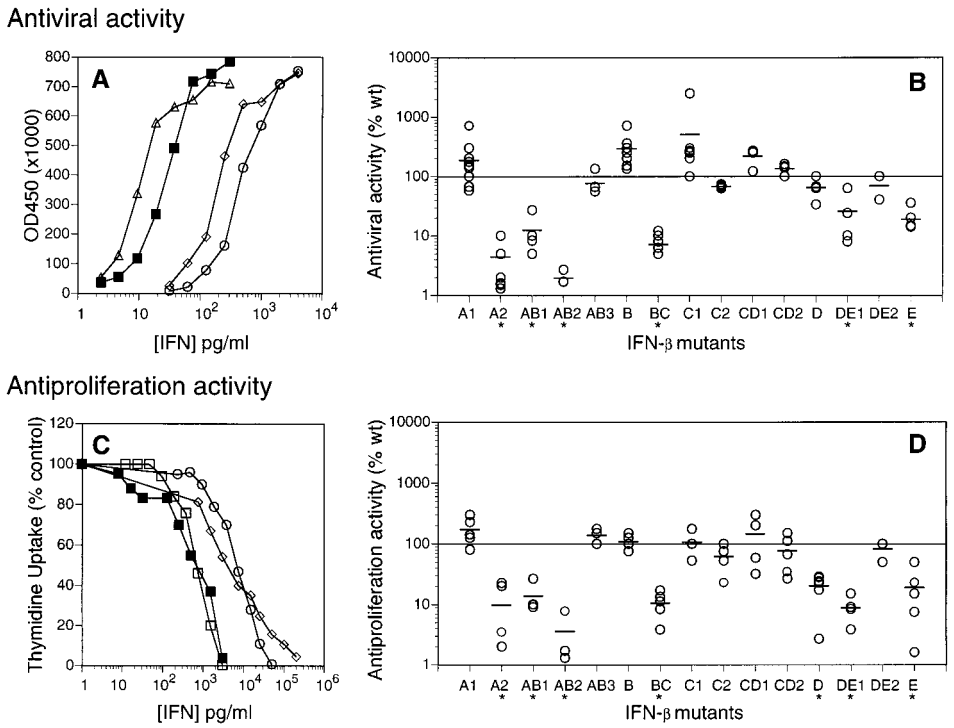

FIGURE 3: Antiviral and antiproliferation activities of mutants A1−E. (A) Representative dose−response data from the antiviral assay for wt his-IFN-β (filled squares) and for mutants AB1 (circles), C1 (triangles), and E (diamonds). Each data point represents the mean of triplicate measurements. Antiviral activities were determined by interpolating the dose−response data to estimate the concentration of wt or mutant his-IFN-β protein that resulted in 50% cell survival. In this assay, wt his-IFN-β gave a mean antiviral activity of 21 pg/mL (range 2.5−61 pg/mL; $n = 19$). (B) Antiviral activity data for all mutants, expressed as a percentage of the activity found for wt his-IFN-β in the same experiment. Each data point represents the activity, relative to wt his-IFN-β, of a given mutant measured in a given experiment. The horizontal bars show the mean antiviral activity for each mutant, averaged over all experiments. Asterisks indicate those mutants showing activity at least 2-fold lower than that of wt his-IFN-β with a statistical significance of $p < 0.01$. (C) Dose−response data from the antiproliferation assay for wt his-IFN-β (filled squares) and for mutants AB1 (circles), C1 (open squares), and E (diamonds). Data points represent the mean of duplicate measurements. Antiproliferation activities were determined by interpolating the dose−response data to estimate the concentration of wt his-IFN-β or mutant protein that gave 50% growth inhibition. In this assay, wt his-IFN-β gave a mean antiproliferation activity of 230 pg/mL (range 70−600 pg/mL; $n = 6$). (D) Antiproliferation activity data for all mutants, expressed as a percentage of the activity found for wt his-IFN-β in the same experiment. Each data point represents the activity, relative to wt his-IFN-β, of a given mutant measured in a given experiment. The horizontal bars show the mean antiproliferation activity for each mutant, averaged over all experiments. Asterisks indicate those mutants showing activity at least 2-fold lower than that of wt his-IFN-β with a statistical significance of $p < 0.01$. Numerical values for the mean antiviral and antiproliferation activities of each mutant, together with the number of replicate measurements and the statistical significance of the difference from wt activity, are given in the Supporting Information.

respective mean antiviral activities. However, the experimental uncertainty in the antiviral and antiproliferation activities (Figure 3B,D) is too large to definitively establish whether these relatively modest deviations from the line are meaningful. The correlation shown in Figure 4 therefore indicates that, for the most part, the mutations have quantitatively rather similar effects on activities in these two assays which measure distinct cellular responses to activation of the type I IFN receptor.

Mutational Effects on Binding to the Type I IFN Receptor on Daudi Cells and to Ifnar2-Fc. A FACS-based binding assay, using the blocking anti-ifnar1 mAb EA12 (*40*) as a probe for free receptor, was developed to determine the affinity of the mutants for binding to the type I IFN receptor on Daudi Burkitt's lymphoma cells. Using this method, described under Materials and Methods, recombinant human IFN-β-1a gave binding curves which yielded apparent K_D values in the range of published values for IFN-β binding to Daudi cells [$(2-3) \times 10^{-10}$ M] (*21, 22*). Interestingly, the average K_D value measured for wt his-IFN-β [$K_D = (3.8 \pm 1.6) \times 10^{-9}$ M] was reproducibly found to be approximately 20-fold higher than that measured for untagged recombinant IFN-β-1a. Thus, although the presence of the N-terminal his-tag extension in wt his-IFN-β had very little effect on the functional activity of the molecule in antiproliferation or antiviral assays, it did appear to weaken receptor binding to some degree. This result, which initially seems counterintuitive, suggests that the affinity of IFN-β for its receptor exceeds the threshold affinity that is required for full activity, as has recently been proposed for human growth hormone binding to its receptor (*47*). The data suggest that wt his-IFN-β, though possessing somewhat reduced affinity for its receptor, still binds strongly enough to approach or exceed the affinity required for full functional activity.

Figure 5A shows binding curves measured for wt his-IFN-β and for three of the mutants in the Daudi cell receptor binding assay. Figure 5B shows the receptor binding affinities measured for each of the mutants in similar experiments; the results are expressed as a percentage of the affinity measured for wt his-IFN-β in the same experiment. Binding affinities for each mutant were measured in at least three separate experiments, using conditioned media from at least two separate transfections. The mean binding affinity for each mutant is shown as a horizontal bar. Figure 5B shows that, for most mutants, the data were highly reproducible between experiments. However, a few of the mutants (notably A1,

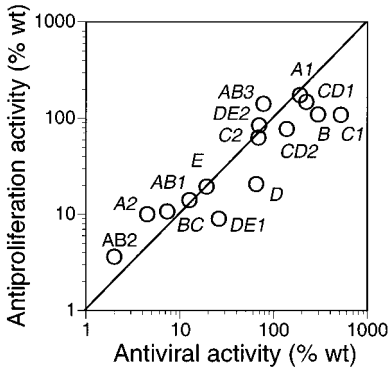

FIGURE 4: Quantitative comparison of the effects of the mutations in mutants A1−E on the antiviral and antiproliferation activities of IFN-β. Antiproliferation activity (from Figure 3B) is shown plotted as a function of antiviral activity (from Figure 3D), for the set of mutants A1−E. In both cases, activity is expressed as a percentage of the activity seen for wt his-IFN-β. Each data point represents the mean antiproliferation and antiviral activities observed for an individual his-IFN-β mutant protein. The identity of each mutant is indicated near the corresponding data point. The solid line has a slope of 1, and represents the relationship expected if, in all cases, mutations had identical effects on activity in both functional assays.

A2, AB2, and C1) showed large experiment-to-experiment variations in the measured K_D values (Figure 5B). We do not know the origins of the variability seen with these few mutants, though control experiments allowed us to rule out as causes any unusual instability of these particular protein preparations or any general instability in the assay. Importantly, however, statistical analysis of the data for these four mutants verified that the reduction in receptor binding affinity observed for mutants A2 and AB2 is highly statistically significant ($p = 1.1 \times 10^{-5}$ and 1.8×10^{-4}, respectively; see Supporting Information) despite the scatter in the data.

The results in Figure 5B show that mutants A1, AB3, C1, CD1, CD2, DE1, and DE2 each displayed an affinity for binding to the cell surface receptor that was at least as high as the affinity measured for wt his-IFN-β. Indeed, several of these mutants—notably A1, C1, CD2, DE1, and DE2—appeared to bind with substantially higher affinities than that of wt his-IFN-β, closer to the affinity seen for untagged recombinant IFN-β-1a. In contrast, mutants A2, AB1, AB2, B, BC, C2, D, and E displayed receptor binding affinities that were from 2- to 200-fold lower than that of wt his-IFN-β. These results show that mutations in parts of the *A* helix, the *AB* loop, and the *B*, *C*, *D*, and *E* helices caused significant reductions in receptor binding affinity, whereas mutations in other parts of the *A* and *C* helices, and in the *CD* and *DE* loops, did not affect receptor binding. Mutations in the regions defined by mutants AB3 and CD1 resulted in binding affinities that were similar to that of wt his-IFN-β, but lower than that of untagged recombinant IFN-β-1a. In these cases, we cannot rule out the possibility that modest effects on receptor binding exist and are being masked by effects on binding caused by the his-tag itself. Unlike mutant D, which showed only a small (though significant) decrease in binding affinity, neither AB3 nor CD1 showed any reduction in functional activity compared to wt his-IFN-β (Figure 3).

To further dissect receptor interactions, the mutants were evaluated in an ELISA measuring their ability to bind to ifnar2-Fc. The EC_{50} values measured in this assay probably do not reflect actual affinities for binding to ifnar2-Fc, because detection involves multiple wash steps and prolonged incubations during which dissociation or reequilibration of IFN-β binding may occur (a problem that the Daudi cell binding assay format avoids). Despite this limitation, this binding assay can be used to provide a useful qualitative indication of which mutations cause a substantial reduction in binding to ifnar2-Fc. As was seen in the Daudi cell receptor binding assay, wt his-IFN-β displayed an EC_{50} value in this assay which, at $\sim 2 \times 10^{-8}$ M, was ~10-fold higher than the value measured for untagged recombinant IFN-β-1a (data not shown).

Figure 5C shows representative ifnar2-Fc binding curves measured for wt his-IFN-β and for three mutants, two of which show binding similar to that seen for wt his-IFN-β and one of which (mutant E) shows no detectable binding to ifnar2-Fc at concentrations up to 1 μM, 500 times higher than the EC_{50} value for wt his-IFN-β. Figure 5D shows EC_{50} values for each of the mutants, expressed as % wt his-IFN-β control; the average result for each mutant is shown as a horizontal bar. The mutants clearly fall into two groups. Mutants A1, AB3, B, BC, C1, C2, CD1, CD2, D, DE1, and DE2 all show EC_{50} values for binding to ifnar2-Fc that fall at or between the value seen for wt his-IFN-β and the ~10-fold higher affinity seen for untagged recombinant IFN-β-1a. In contrast, mutants A2, AB1, AB2, and E showed no detectable binding to ifnar2-Fc in this assay (Figure 5D), suggesting that mutations in these sites substantially weaken binding to ifnar2-Fc. These data suggest that the weakened affinities for binding to the receptor on Daudi cells that was measured for the mutants A2, AB1, AB2, and E (Figure 5B) result from substantially reduced binding to the ifnar2 receptor component of the receptor. Mutants B and C2 also showed reduced affinities for binding to the receptor on Daudi cells, but clearly retained their affinity for ifnar2-Fc. The regions affected by these mutations lie in the *B* and *C* helices, on the opposite face of the molecule to the ifnar2 binding regions. These regions of the molecule are therefore most likely involved in binding to ifnar1. Mutants AB3, BC, D, and DE1 bind ifnar2-Fc comparably to wt his-IFN-β, but more weakly than the untagged IFN-β-1a. Because of the possibility in these cases that mutational effects on binding are being masked by effects due to the his-tag, we cannot definitively say whether these four mutants are also involved in binding to ifnar1.

Mapping Mutational Effects on Receptor Binding and on Functional Activity onto the Structure of IFN-β. Figure 6 summarizes the binding and activity data from Figures 3 and 5, projected onto the three-dimensional structure of human IFN-β. The space-filling representations of the protein structure shown in Figure 6 panels a−d are based on the crystallographic coordinates (*34*), and show the molecule in two orientations related by a 180° rotation to show both "front" and "back". The data are color-coded as follows: portions of the molecule colored green indicate regions in which mutations resulted in no significant effect (i.e., <2-fold reduction) on activity or binding affinity in a given assay; regions colored blue indicate a reduction in activity or binding affinity of from 2- to 5-fold; and regions colored red indicate that mutations in these sites reduced activity or binding affinity by ≥5-fold. Regions of the molecule colored yellow were not altered by the mutations (Figure 1).

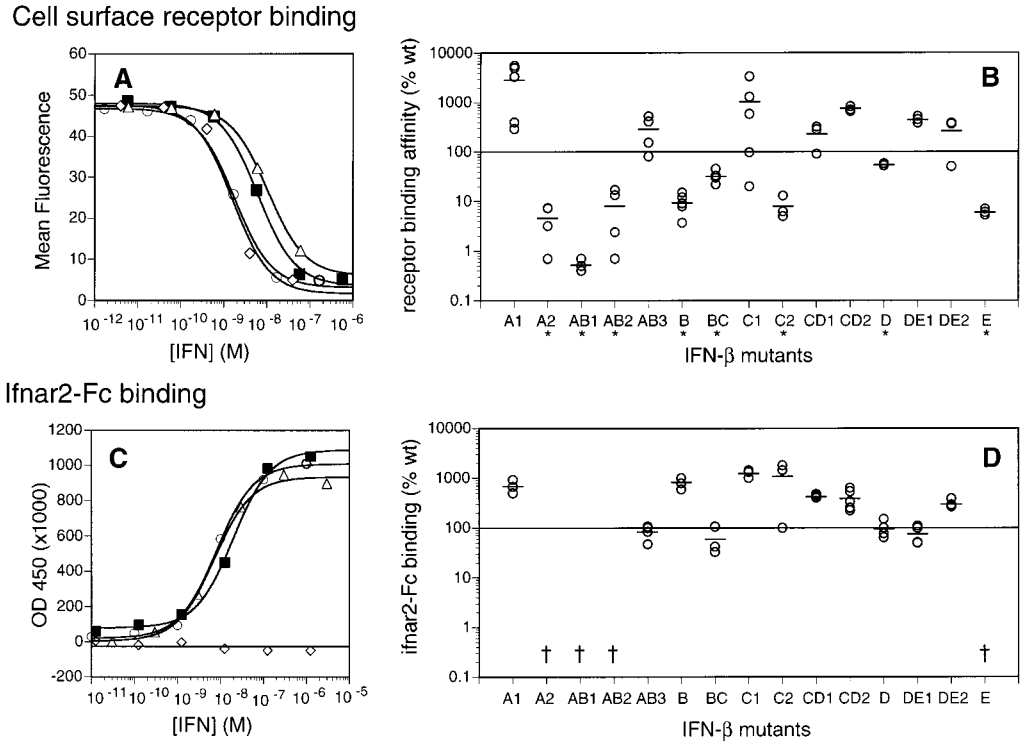

FIGURE 5: Cell surface receptor binding and ifnar2-Fc binding properties of mutants A1−E. (A) Representative data from the Daudi cell receptor binding assay for wt his-IFN-β (filled squares) and for mutants DE1 (diamonds), DE2 (circles), and D (triangles). Receptor binding affinities were taken as the IC_{50} values from the best fits of the data to a four-parameter equation, shown by the solid lines. In this assay, wt his-IFN-β gave a K_D for binding to the receptor on Daudi cells of $(3.8 \pm 1.6) \times 10^{-9}$ M ($n = 20$), where the uncertainty limit represents the standard deviation between independent experiments. (B) Binding affinities for the binding of mutants A1−E to the receptor on Daudi cells, expressed in each case as a percentage of that measured for wt his-IFN-β in the same experiment. Each data point represents the receptor binding affinity, relative to wt his-IFN-β, found for a given mutant in a given experiment. The horizontal bars show the mean affinity for each mutant, averaged over all experiments. Asterisks indicate those mutants showing binding affinities that were at least 2-fold lower than that of wt his-IFN-β with a statistical significance of $p < 0.01$. (C) Ifnar2-Fc binding data for wt his-IFN-β (filled squares) and for mutants DE2 (circles), CD (triangles), and E (diamonds). EC_{50} values for Ifnar2-Fc binding were determined from the best fits of the data to a hyperbolic binding equation, shown by the solid lines. (D) Ifnar2-Fc binding activities for all mutants, expressed as a percentage of the binding activity found for wt his-IFN-β in the same experiment [i.e., % binding $= EC_{50}(\text{wt})/EC_{50}(\text{mutant}) \times 100$]. Each data point represents the result found for a given mutant in a given experiment. The horizontal bars show the mean binding activity for each mutant, averaged over all experiments. The dagger symbol (†) indicates that mutants A2, AB1, AB2, and E showed no detectable ifnar2-Fc binding when tested at IFN concentrations up to 1 μM, 500-fold greater the EC_{50} value measured for wt his-IFN-β.

Figure 6a shows the activity data obtained for each mutant in the antiviral assay, color-coded and mapped onto the appropriate surface regions of a structural model of IFN-β. Figures 6b, 6c, and 6d show similar images representing the results of the antiproliferation, cell surface receptor binding, and ifnar2-Fc binding assays, respectively. Data from a number of additional point mutants are also included in Figure 6. The effects of the individual point mutations R27A, R35A (*AB* loop), and K123A (*D* helix) on the antiviral activity of IFN-β have been reported previously (*42*), and are included in Figure 6a. In addition, mutants H93A/H97A and H121A, located in the *C* and *D* helices, respectively, which substitute the zinc-chelating histidine residues in the zinc-mediated IFN-β-1a dimer that was observed in the crystal structure (*34*), were constructed and assayed for antiviral activity and for binding to the receptor on Daudi cells and to ifnar2-Fc (data not shown). The activities of these mutants were indistinguishable from that of wt his-IFN-β in these assays, and so H93A, H97A, and H121A are shown in green in Figures 6a, 6c, and 6d.

The most striking feature of Figure 6 is that mutations in the regions corresponding to mutants A1, AB3, C1, CD1, and CD2, which together cover almost half of the molecular surface proximal to both the N- and C-termini, had no measurable effect on binding or activity in any of the four assays. These regions of the molecule appear to play no significant role in receptor binding or activation. In contrast, four regions of the molecule, altered in mutants A2, AB1, AB2, and E, are colored red in all four images, indicating that mutations in these regions of the molecule caused at least a 5-fold decrease in activity or binding affinity in all assays. Figure 6d indicates that these four regions together define a contiguous patch of the molecular surface, and that only mutations in these regions caused any detectable reduction in binding to ifnar2-Fc. We therefore conclude that the region defined by mutants A2, AB1, AB2, and E constitutes the ifnar2 binding site on IFN-β. On the opposite face of the molecule the situation appears more complex. Mutations in the regions corresponding to mutants B, BC, C2, D, and DE1 all affect activity in one or more of the assays, and these regions too can be seen to form a contiguous patch on the molecular surface. However, the effects of any given mutation in this region appear to be quantitatively different in the different assays, and no clear correlation exists between effects on binding affinity and on biological activity. Since mutations on this face of the molecule have no detectable effect on binding to ifnar2, though several affect binding to the receptor on Daudi cells,

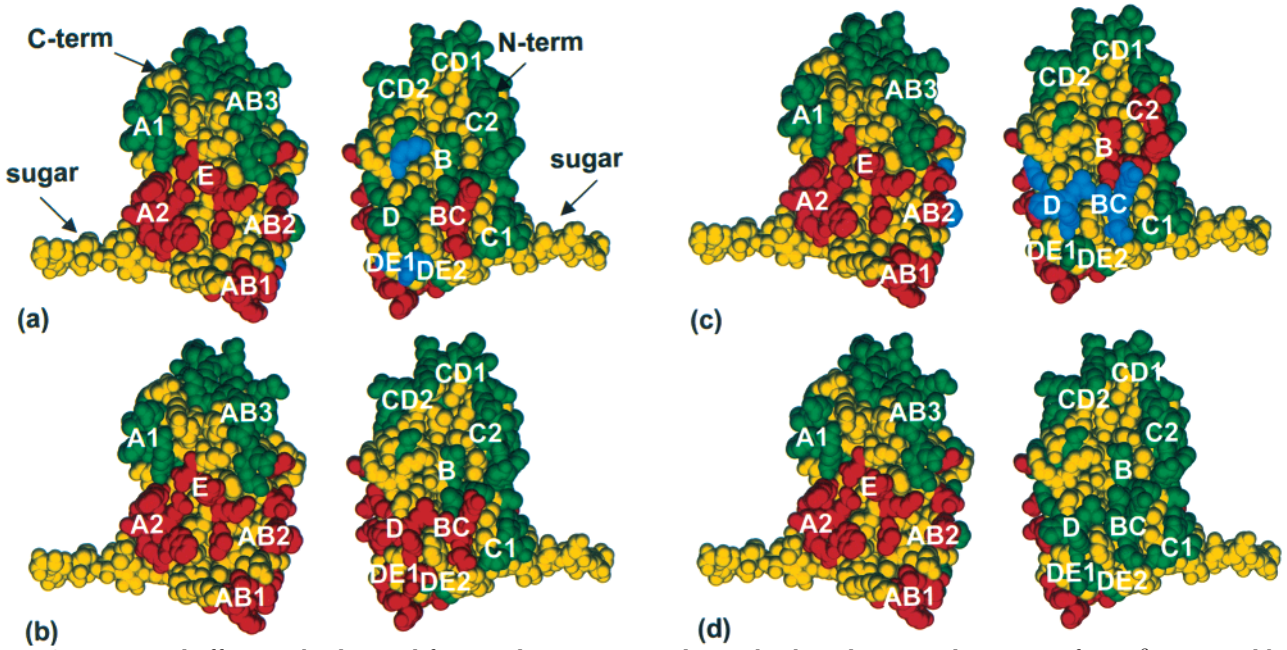

FIGURE 6: Mutational effects on binding and functional activity mapped onto the three-dimensional structure of IFN-β. Front and back views of a space-filling representation of the crystal structure of IFN-β, color-coded to summarize the effects of the mutations on the antiviral (a), antiproliferation (b), receptor binding (c), and ifnar2-Fc binding (d) properties of his-IFN-β. The magnitude of the mutational effect on activity in a given assay is color-coded as follows: For panels a−c, residues that, when mutated, resulted in no loss of activity (i.e., <2-fold reduction) in a given assay are colored green; residues that, when mutated, caused a reduction in activity of 2−5-fold are colored blue; residues that, when mutated, caused a ≥5-fold loss in activity are colored red. In panel d, mutations that caused a complete loss of ifnar2-Fc binding in the assay are colored red; mutations that caused no detectable effect on ifnar2-Fc binding are colored green. In all four panels, portions of the molecule colored yellow were not altered by the mutations (see Figure 1). The positions of the protein's N- and C-termini are indicated by arrows, as is the position of the carbohydrate on Asn80. In addition to the 15 alanine-substitution mutants A1−E, the effects of mutating residues R27, R35, and K123 on the antiviral activity of IFN-β have been reported previously (*42*), and are included in panel a. Two additional his-IFN-β mutants, H93A/H97A and H121, were analyzed in three of the four assays and in all cases gave wild-type activity. These three histidine residues are therefore colored green in panels a, c, and d. Figures were prepared using RIBBONS (*63*).

it is likely that this region of the molecule exerts its effect through interaction with ifnar1.

DISCUSSION

Identification of Human IFN-β Receptor Binding and Functional Domains. Correlating the assay data from Figures 3 and 5 with the location of the corresponding mutations on the three-dimensional structure of IFN-β led to the identification of two distinct receptor binding regions on opposite faces of the IFN-β molecule. One region, defined by mutations in the *A* helix, the *AB* loop, and the *E* helix, was found to be critical for ifnar2 binding. Each of the four mutants (A2, AB1, AB2, E) that affected this region of the protein also showed a substantial (i.e., >10-fold) decrease in receptor binding affinity and proportionate reductions in functional activities (Figure 6). This region of the molecule was concluded to comprise the ifnar2 binding site on IFN-β. A second receptor-interacting region, on the opposite face of the molecule, was also identified. Mutations in this region, which comprises portions of the *B*, *C*, and *D* helices and parts of the *BC* and *DE* loops, also showed effects on receptor binding, antiviral activity, and/or antiproliferation activity. In the case of mutants B and C2, binding to ifnar2 clearly was unaffected, suggesting that their substantially reduced affinity for the receptor on Daudi cells can be attributed to altered interactions with ifnar1. The mutations in BC, D, and DE1 are adjacent to those in B and C2, and these three mutants also demonstrated reduced activity in one or both functional assays while retaining ifnar2 binding properties similar to that of wt his-IFN-β. It is therefore likely that the region of the molecular surface defined by mutants B, BC, C2, D, and DE1 comprises the ifnar1 binding site on IFN-β. Mutations within this putative ifnar1 binding site tend to have disproportionate effects on receptor binding and activity. For example, mutants B and C2 showed approximately wild-type levels of activity in both functional assays, but demonstrated a reduction in receptor binding affinity of >10-fold, comparable to that seen in the four ifnar2 binding site mutants which showed large reductions in activity in both functional assays. Mutant BC showed reductions in activity that were large relative to the effect of the mutations on receptor binding affinity. In contrast, mutant DE1 showed marked reductions in activity in both functional assays, but showed no reduction in receptor binding affinity. Thus, interactions with ifnar1 appear to affect binding and activity in more complex ways than was seen for mutations in the ifnar2 binding site.

The locations of the ifnar1 and ifnar2 binding sites on IFN-β deduced from our data can be compared to literature data. Previous mutagenesis data on IFN-β (*42*), interpreted in light of the X-ray crystal structure of IFN-β-1a (*34*), have identified R35 in the *AB* loop, K123 in the *D* helix, and sites on the *C* helix (N84, Y92) as being involved in functional interactions with the receptor. Moreover, mAbs that block the function of IFN-β in vitro in activity assays have been mapped to epitopes that defined two receptor binding regions on opposite faces of the molecule, one of which was shown to comprise residues within the region of amino acids 40−

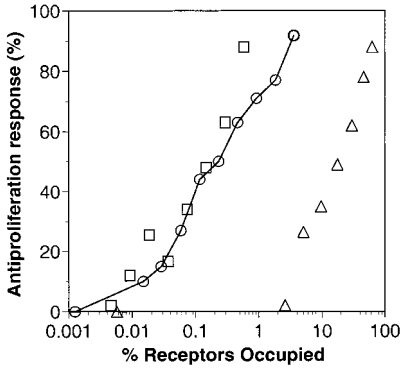

FIGURE 7: Quantitative differentiation between mutational effects on receptor binding and on antiproliferation activity. Dose−response data from representative antiproliferation assays performed with wt his-IFN-β (circles) and mutants A2 (squares) and DE1 (triangles), in which the concentration axis is expressed in terms of % receptors occupied. The percentage of receptors occupied at each concentration of wt or mutant his-IFN-β was calculated using a single site (i.e., hyperbolic) binding equation and the appropriate receptor binding affinity for each mutant, from Figure 5B. Both antiproliferation activity and receptor binding were measured using Daudi cells. The percent receptor occupancy required to achieve half-maximal antiproliferation response is given Table 1, for wt his-IFN-β and for those mutants that showed significantly reduced antiproliferation activity.

53 of the *AB* loop and *B* helix (*45*). All of these findings are in good agreement with our results. For IFN-α, solvent-exposed residues on the portions of the *AB* loop, the *DE* loop, and *B* and *E* helices, identified as functionally important residues (reviewed in *36*), have been suggested to be important for receptor interactions (*33*), and the *C* helix has been implicated in interactions between human IFNs-α1 and -α8 with ifnar1 (*48*). However, there is evidence that, despite the overall involvement of roughly similar regions of the molecule, the specific regions that contact ifnar1 and ifnar2 may be different for IFN-α subtypes than those defined herein for human IFN-β-1a. We observed that the solvent-exposed residues of IFN-β shown by this study to interact with ifnar2 are not well-conserved between IFN-β and IFN-α. This observation is in line with a model proposed by Mogensen et al. (*31*) in a recent review, in which the authors utilized structures of IFN-α2 and IFN-β to demonstrate that striking homologies exist between residues that lie on opposite surfaces of these molecules, and proposed that IFNs-α2 and -β would present quite different solvent-exposed residues to ifnar1 and ifnar2.

Differentiating Mutational Effects on Receptor Activation from Effects on Receptor Binding. Mutations in IFN-β can potentially affect the activity of the molecule in two distinct ways: by altering its affinity for the receptor, or by affecting its ability to trigger receptor activation once it has bound. These two kinds of effects can be quantitatively differentiated and thus separately analyzed as shown in Figure 7. Figure 7 shows dose−response data from the antiproliferation assay for wt his-IFN-β and for mutants A2 and DE1, but with the concentration axis expressed not in units of molarity but instead in terms of the percentage of receptors occupied at each IFN concentration tested. Percent receptor occupancy at each IFN concentration was calculated using the receptor binding affinities measured for each IFN-β mutant (Figure 5B), as described in the legends to Figure 7 and Table 1. The receptor binding affinities from Figure 5B are directly applicable to data from the antiproliferation assay because both measurements were made using identical Daudi cells. By plotting the antiproliferation dose−response data as shown in Figure 7, differences in receptor binding affinity between different forms of IFN-β are factored out, and the data report directly on the ability of each IFN mutant to induce a functional response once bound to the receptor.

Table 1: Levels of Receptor Occupancy Required To Achieve a Half-Maximal Response in the Antiproliferation Assay, for wt his-IFN-β and Mutants That Showed Significantly Attenuated Antiproliferation Activity

mutant	antiproliferation act.[a] (% wt)	% receptor occupancy at half-max response[b]
wt his-IFN-β	100	0.3
A2	4.7	0.14
AB1	14	0.012
AB2	3.6	0.70
BC	11	0.94
D	20	0.82
DE1	9.1	13
E	19	0.1

[a] Mean EC_{50} values measured in the antiproliferation assay, expressed as a percentage of the EC_{50} value for wt his-IFN-β (data from Figure 3D). [b] Percentage of receptors occupied at a concentration of each IFN-β mutant equal to its EC_{50} value in the antiproliferation assay. Receptor occupancy was calculated using a single site (i.e., hyperbolic) binding equation and the K_D value for wt his-IFN-β or each mutant measured in the Daudi cell receptor binding assay (Figure 5A,B). Full dose−response curves plotted as a function of percent receptors occupied are shown in Figure 7 for wt his-IFN-β and for mutants A2 and DE1.

Figure 7 shows that wt his-IFN-β brings about a 50% maximal antiproliferative response on Daudi cells when present at a concentration at which only ∼0.3% of receptors are occupied. It appears, therefore, that this response to IFN-β is maximally stimulated upon activation of only a very small number of receptors. Figure 3D shows that mutant A2 has an antiproliferation activity that is reduced ∼10-fold compared to wt his-IFN-β. However, Figure 7 shows that, for a given level of receptor occupancy, these two proteins are equally effective at inducing this functional response. The data in Figure 7 show, therefore, that the low activity of A2 is solely due to its reduced affinity for binding to the receptor (Figure 5B); once bound to the receptor, its ability to induce an antiproliferation response is unimpaired. Comparable results are seen if data for two other ifnar2 site mutants, AB2 and E, are plotted in the same way (summarized in Table 1). In contrast, the antiproliferation activity of mutant DE1 is also ∼10-fold lower than that of wt his-IFN-β, but unlike A2 its binding to the receptor is not correspondingly weakened. Figure 7 shows, therefore, that mutant DE1 achieves a 50% maximal antiproliferation response only when present at concentrations at which it is occupying ∼13% of receptors. This result implies that, once bound to the receptor, DE1 is ∼40 times less effective than wt his-IFN-β or mutant A2 at activating the receptor to trigger an antiproliferative response. These findings suggest that the binding energy derived from interactions of the sites defined by mutants A2, AB2, and E with ifnar2 is fully expressed in the observed receptor binding affinity, and thus imply that the main function of interactions with ifnar2 is to bind IFN-β to the receptor by stabilizing the resulting complex. In contrast, the binding energy derived from interaction of the DE1 region with ifnar1 is not expressed in the observed

binding affinity; hence, the affinity is not reduced upon mutation at this site. Instead, the binding energy is utilized to bring about signaling, presumably by selectively stabilizing activated states of the receptor. Consideration of receptor activation in terms of the generation of binding energy, and its expression in the observed binding affinity or its utilization to bring about receptor activation, is closely analogous to the well-developed theory of the utilization of binding energy by enzymes to achieve catalysis (*49*).

Mutations that decrease receptor activation much more than they reduce binding have been reported for other cytokines such as growth hormone (*50*), erythropoietin (*51*), and IL-4 (*52*). In these cases, the effects were due to a decreased ability to recruit a second receptor chain after binding of ligand to the first chain. The question of whether a mechanism of ligand-induced receptor dimerization plays a role in activation of the type I IFN receptor has not yet been definitively answered. However, the complex pattern of variations between effects on receptor binding and on functional activity that is seen for mutations in the proposed ifnar1 binding site (see Figure 6a−c) suggests that a more complicated mechanism is at work. This notion is in keeping with published data that imply that there is an important allosteric component to activation of the type I IFN receptor (*53, 54*). Assuming that the variations in behavior seen in Figure 7 are largely due to effects on the distribution of receptor states that exists at binding equilibrium, and that purely kinetic explanations can be ruled out (*47*), comparison of the data for A2 and DE1 suggests that activation of the type I interferon receptor by different IFN-β mutants can give rise to distinct activated states of the receptor which differ in the efficiency with which they induce a given functional response. Such a result might be achieved if the receptor is able to adopt multiple distinct activated conformations that differ in the efficiency with which they promote a particular functional response. Alternatively, the data can be interpreted in terms of a single activated state, if the activity differences between the mutants result from quantitative differences in the equilibrium distribution between active and inactive states that is induced upon IFN binding. In either case, the data suggest that activation of the type I IFN receptor contains an important allosteric component. The effects of our IFN-β mutants on the nature and distribution of activated receptor states, which we infer from Figure 7, may provide a model for how engagement of the type I IFN receptor by different type I IFNs can give rise to distinct functional responses.

Relevance of IFN-β Dimer Formation for Receptor Binding and Activity. Human IFN-β-1a was observed to crystallize as noncovalent dimers, in which residues H93 and H97 in one molecule and H123 in the neighboring molecule participate in the dimer contact through their chelation of a bridging zinc ion (*34*). Interestingly, IFN-α2b was also found to crystallize as a zinc-mediated dimer, though with a quite different orientation between its component monomers (*33*). Though zinc has not been implicated in the function of either of these interferons, it is known to be involved in the binding of human growth hormone to the prolactin receptor (*55*), and has been reported to affect the binding of insulin-like growth factor to its receptor (*56*). Moreover, there are reports that suggest that rare earth salts can enhance IFN-β receptor binding and functional activity (*57*). To test whether the zinc-mediated dimerization of IFN-β that is observed crystallographically is important for function, we prepared two additional IFN-β mutants in which the zinc-chelating histidine residues from one or the other face of the molecule were replaced by alanine residues. These two mutants, H123A and H93A/H97A, both displayed activity comparable to wt his-IFN-β in antiviral assays, in cell surface receptor binding, and in ifnar2-Fc binding assays (data not shown). Moreover, additional points of contact between the IFN-β molecules in the crystallographically observed IFN-β dimers fall in regions of the molecule that are altered in mutants A1, C2, and CD1, all of which retained activities identical to wt his-IFN-β in functional assays. These results suggest that the dimers seen in the crystal structure of IFN-β represent a crystallization artifact that is not relevant to function.

Receptor Binding Domains of IFN-β: Comparison with Human Growth Hormone. The extensive high-resolution structural and functional studies that have been performed on human growth hormone (hGH), using cell surface expressed receptor (GH-R) or a soluble receptor construct known as hGHbp, have elucidated detailed molecular recognition principles likely to be generally applicable to the helical cytokine families of ligands and receptors (*58*). While the sequence homology between hGH and IFN-β is rather low, the four-helix bundle core is a well-conserved structural feature, and the overall three-dimensional folds of hGH and IFN-β are therefore quite similar. However, while hGH acts through a receptor comprised of two identical receptor chains, the receptor for IFN-β comprises distinct ifnar1 and ifnar2 components. For the type I IFN receptor, the extracellular, cytokine binding domains are structurally homologous to each other and to GH-R, each being comprised of fibronectin type (FN)-III repeats. Elegant alanine-scanning mutagenesis experiments coupled with receptor binding and crystallographic studies (*59*−*61*) have clearly defined the residues that comprise the high-affinity (site 1) and low-affinity (site 2) receptor binding sites on hGH, and have pinpointed the subset of contact residues that contribute most to binding energy with the receptor. In light of the conserved structural features of helical cytokines and their respective receptors, we examined whether the IFN-β mutational data described above, when compared to data for hGH, might point to similarities and differences in how these two helical cytokines engage their respective receptors. A superimposition of the murine IFN-β structure (1 rmi) on the hGH structure (1 huw), based on structural rather than sequence similarities, is available in the FSSP database (*62*). Our examination of this superimposition showed that the ifnar2 binding site on IFN-β closely coincides with the high-affinity receptor binding site (site 1) on hGH. Noteworthy is the presence of several solvent-exposed hydrophobic residues (F15, W22, L32, and V148) at the ifnar2 binding surface of IFN-β. These hydrophobic residues are likely to impart binding energy in an analogous manner to the critical hydrophobic residues that are clustered at the center of high-affinity site 1 of hGH. For both cytokines, therefore, the interaction site that generates the bulk of the binding affinity with the receptor involves structurally analogous regions of the protein surfaces. In contrast, the putative ifnar1 binding site, which consists of helices *B*, *C*, and *D* on the opposite face of the IFN-β molecule, does not coincide with the low-affinity site (site 2) on hGH. This difference in the structural

details of receptor engagement by IFN-β compared to hGH may be related to the fact that ifnar1 contains four FN-III repeats in its extracellular domain rather than the two found in GH-R and in ifnar2. This structural feature may allow binding geometries between IFN-β and ifnar1 that are unavailable for hGH/GH-R interactions. Finally, the fairly large areas of the IFN-β protein surface that were identified herein to be involved in interactions with the receptor appear to differ from the smaller, more focal, receptor interaction sites that were identified on growth hormone (*58*−*60*) and some other helical cytokines (*51, 52*). However, this apparent difference may simply be a consequence of the fact that, in the current study, surface residues were mutated not singly but in groups. A higher resolution scan in which the functionally important regions of the molecule were probed by single point mutations might therefore give a picture of the receptor interaction sites that more closely resembles the compact sites seen in other cases. Such a high-resolution scan would also allow some of the quantitative conclusions we have inferred from our data to be tested in more detail, shedding additional light on exactly how binding of IFN-β to its receptor brings about receptor activation and functional responses.

ACKNOWLEDGMENT

We express appreciation to Margot Brickelmaier and Cindy Su for their valuable contributions to developing the FACS-based Daudi cell binding assay for IFN. We are grateful to Dr. Philip Redlich and Prof. Sidney Grossberg for the gift of anti-IFN-β mAbs. We also thank our colleagues and collaborators Drs. Darren Baker, Alan Gill, Werner Meier, Rich Cate, Marie Green, Chris Borysenko, Ann Boriak-Sjodin, K. Erik Mogensen, and Gilles Uzé for helpful discussions.

SUPPORTING INFORMATION AVAILABLE

Statistical analysis of the mean activity values for his-IFN-β mutants analyzed in functional and receptor binding assays (p values) (2 pages). This material is available free of charge via the Internet at http://pubs.acs.org.

REFERENCES

1. Stewart, W. E., II (1981) in *The Interferon System*, pp135−156, Springer Verlag, New York.
2. Tyring, S. K. (1995) *Am. J. Obstet. Gynecol. 172*, 1350−1353.
3. Pestka, S., Langer, J. A., Zoon, K. C., and Samuel, C. E. (1987) *Annu. Rev. Biochem. 56*, 727−745.
4. Diaz, M. O., Pomykala, H. M., Bohlander, S. K., Maltepe, E., Malik, K., Brownstein, B., and Olopade, O. I. (1994) *Genomics 22*, 540−552.
5. Weissmann, C., and Weber, H. (1986) *Res. Mol. Biol. 33*, 251−300.
6. Uzé, G., Lutfalla, G., and Gresser, I. (1990) *Cell 60*, 225−234.
7. Novick, D., Cohen, B., and Rubinstein, M. (1994) *Cell 77*, 391−400.
8. Domanski, P., Witte, M., Kellum, M., Rubinstein, M., Hackett, R., Pitha, P., and Colamonici, O. (1995) *J. Biol. Chem. 270*, 21606−21611.
9. Lutfalla, G., Holland, S. J., Cinato, E., Monneron, D., Reboul, J., Rogers, N. C., Smith, J. M., Stark, G. R., Gardiner, K., Mogensen, K. E., Kerr, I. M., and Uzé, G. (1995) *EMBO J. 14*, 5100−5108.
10. Bazan, J. F. (1990) *Proc. Natl. Acad. Sci. U.S.A. 87*, 6934−6938.
11. Uzé, G., Lutfalla, G., and Mogensen, K. E. (1995) *J. Interferon Cytokine Res. 15*, 3−26.
12. Walter, M. R., Windsor, W. T., Nagabhushan, T. L., Lundell, D. J., Lunn, C. A., Zauodny, P. J., and Narula, S. K. (1995) *Nature 376*, 230−235.
13. Harlos, K., Martin, D. M. A., O'Brian, D. P., Jones, E. Y., Stuart, D. I., Polikarpov, I., Miller, A., Tuddenham, E. G. D., and Boys, C. W. G. (1994) *Nature 370*, 662−666.
14. Kotenko, S. V., Krause, C. D., Izotova, L. S., Pollack, B. P., Wu, W., and Pestka, S. (1997) *EMBO J. 16(*19), 5894−5903.
15. Velazquez, L., Fellous, M., Stark, G. R., and Pellegrini, S. (1992) *Cell 70*, 313−322.
16. Colamonici O., Yan, H., Domanski, P., Handa, R., Smalley, D., Mullersman, J., Witte, M., Krishnan, K., and Kotelewski, J. (1994) *Mol. Cell. Biol. 14*(12), 8133−8142.
17. Darnell, J. E., Jr., Kerr, I. M., and Stark, G. M. (1994) *Science 264*, 1415−1421.
18. David, M., Petricoin, E., 3rd, Benjamin, C., Pine, R., Weber, M. J., and Larner, A. C. (1997) *Science 269*, 1721−1723.
19. Fish, E. N., Uddin, S., Korkmaz, M., Majchrzak, B., Druker, B. J., and Platanias, L. C. (1999) *J. Biol. Chem. 274*(2), 571−573.
20. Der, S. D., Zhou, A., Williams, B. R., and Silverman, R. H. (1998) *Proc. Natl. Acad. Sci. U.S.A. 95*(6), 15623−15628.
21. Cohen, B., Novick, D., Barak, S., and Rubinstein, M. (1995) *Mol. Cell. Biol. 15*(8), 4208−4214.
22. Cutrone, E. C., and Langer, J. A. (1997) *FEBS Lett. 404*, 197−202.
23. Lim, J., Xiong, J., Carrasco, N., and Langer, J. A. (1994) *FEBS Lett. 350*, 281−286.
24. Cleary, C. M., Donnelly, R. J., Soh, J., Mariano, T. M., and Pestka, S. (1994) *J. Biol. Chem. 269*, 18747−18749.
25. Cook, J. R., Cleary, C. M., Mariano, T. M., Izotova, L., and Pestka, S. (1996) *J. Biol. Chem. 271*(23), 13448−13453.
26. Fish, E. N., Banerjee, K., and Stebbing, N. (1983) *Biochem. Biophys. Res. Commun. 112*(2), 537.
27. Pfeffer L. M., and Constantinescu, S. N. (1997) in *Interferon Therapy in Multiple Sclerosis* (Reder, A. T., Ed.) Marcel Dekker, Inc., New York.
28. Abramovitch, C., Shulman, L., Ratoviski, E., Harroch, S., Tovey, M., Eid, P., and Revel, M. (1995) *EMBO J. 13*, 5871−5877.
29. Constantinescu, S. N., Croze, E., Murti, A., Wang, C., Basu, L., Hollander, D., Russel-Harde, D., Betts, M., Garcia-Martinez, V., Mullersman, J. E., and Pfeffer, L. M. (1995) *Proc. Natl. Acad. Sci. U.S.A. 92*, 10487−10491.
30. Domanski, P., Nadeau, O. W., Platanias, L. C., Fish, E., and Colamonici, O. R. (1998) *J. Biol. Chem. 273*(6), 3144−3147.
31. Mogensen, K. E., Lewerenz, M., Reboul, J., Lutfalla, G., and Uze, G. (1999) *J. Interferon Cytokine Res. 19*, 1069−1098.
32. Senda, T., Saitoh, S., and Mitsui, Y. (1995) *J. Mol. Biol. 253*, 187−207.
33. Radhakrishnan, R., Walter, L. J., Hruza, A., Reichert, P., Trotta, R. P., Nagabhushan, T. L., and Walter, M. R. (1996) *Structure 4*, 1453−1463.
34. Karpusas, M., Nolte, M., Benton, C. B., Meier, W., and Goelz, S. (1997*) Proc. Natl. Acad. Sci. U.S.A. 94*, 11813−11818.
35. Radhakrishnan, R., Walter, L. J., Subramaniam, P. S., Johnson, H. M., and Walter, M. R. (1999) *J. Mol. Biol. 286*, 151−162.
36. Mitsui, Y., Senda, T., Shimazu, T., Matsuda, S., and Utsumi, J. (1993*) Pharmacol. Ther. 58*, 93−132.
37. Rose, R. E. (1988) *Nucleic Acids Res. 16*(1), 355−364.
38. Osborn, L., Hession, C., Tizard, R., Vassallo, C., Luhowskyj, S., Chi-Rosso, G., and Lobb, R. (1989) *Cell 59*(6), 1203−1211.
39. Chittenden, T., Lupton, S., and Levine, A. J. (1989) *J. Virol. 63*(7), 3016−3025.
40. Goldman, L. A., Zafari, M., Cutrone, E. C., Dang, A., Brickelmeier, M., Runkel, L., Benjamin, C. D., Ling, L. E., and Langer, J. A. (1999) *J. Interferon Cytokine Res. 1*, 15−26.
41. Jost, L. M., Kirkwood, J. M., and Whiteside, T. L. (1992) *J. Immunol. Methods 147*, 153−165.

42. Runkel, L., Pfeffer, L., Lewerenz, M., Monneron, D., Yang, C. H., Murti, A., Pellegrini, S., Goelz, S., Uze. G., and Mogensen, K. E. (1998) *J. Biol. Chem. 273*(14), 8003−8008.
43. Runkel, L., Meier, W., Pepinsky, R. B., Karpusas, M., Whitty, A., Kimball, K., Brickelmaier, M., Muldowney, C., Jones, W., and Goelz, S. E. (1998) *Pharm. Res. 15*(4), 641−649.
44. Redlich., P. N., and Grossberg, S. E. (1990) *Eur. J. Immunol. 20*, 1933−1939.
45. Redlich, P. N., Hoeprich, P. D., Jr., Colby, C. B., and Grossberg, S. E. (1991*) Proc. Natl. Acad. Sci. U.S.A. 88*, 4040−4044.
46. Qin, X.-Q., Runkel, L., Deck, C., deDios, C., and Barsoum, J. (1997) *J. Interferon Cytokine Res. 17*, 355−367.
47. Pearce, K. H., Cunningham, B. C., Fuh, G., Teeri, T., and Wells, J. A. (1999) *Biochemistry 38*(1), 81−89.
48. Uzé, G., Di Marco, S., Mouchel-Vielh, E., Monneron, D., Bandu, M.-T., Horisberger, M. A., Dorques, A., Lutfalla, G., and Mogensen, K. E. (1994*) J. Mol. Biol. 243*, 245−257.
49. Jencks, W. P. (1975) *Adv. Enzymol. Relat. Areas Mol. Biol. 431*, 19−410.
50. Fuh, G., Cunningham, B. C., Fukunaga, R., Nagata, S., Goedell, D. V., and Wells, J. A. (1992) *Science 256*, 677−680.
51. Matthews, D. J., Topping, R. S., Cass, R. T., and Giebel, L. B. (1996) *Proc. Natl Acad. Sci. U.S.A. 93*, 9471−9476.
52. Kruse, N., Shen, B. J., Arnold, S., Tony, H. P., Muller, T., and Sebald, W. (1993) *EMBO J. 12*(13), 5121−5129.
53. John, J., McKendry, R., Pellegrini, S., Flavell, D., Kerr, I. M., and Stark, G. R. (1991) *Mol. Cell. Biol. 11*, 4189−4195.
54. Gauzzi, M. C., Barbieri, G., Richter, M. F., Uze, G., Ling, L., Fellous, M., and Pellegrini, S. (1997) *J. Biol. Chem. 94*(22), 11839−11844.
55. Matthews, D. J., and Wells, J. A. (1994) *Chem. Biol. 1*, 25−30.
56. McCuster, R. H., Kaleko, M., and Sackett, R. L. (1998) *J. Cell. Physiol. 176*, 392−401.
57. Sedmak, J. J., and Grossberg, S. E. (1981) *J. Gen. Virol. 52*, 195−198.
58. Wells, J. A., and de Vos, A. M. (1996) *Annu. Rev. Biochem. 65*, 609−634.
59. Cunningham, B. C., and Wells, J. A. (1989) *Science 244*, 1081−1085.
60. de Vos, A. M., Ultsch, M., and Kossiakoff, A. A. (1992) *Science 255*, 306−312.
61. Clackson, T., Ultsch, M. H., Wells, J. A., and de Vos, A. M. (1998) *J. Mol. Biol. 277*, 1111−1128.
62. Holm L., and Sander, C. (1996) *Science 273*, 595−603.
63. Carson, M. (1997) *Methods Enzymol. 277*, 493−505.

BI991631C